Gyroscopic Stabilization of an Unmanned Bicycle

Harun Yetkin[†], Simon Kalouche[‡], Michael Vernier[†], Gregory Colvin[‡], Keith Redmill[†] and Umit Ozguner[†]

Abstract— **There are two theoretical methods by which a two wheeled vehicle oriented in tandem can be stabilized: dynamic stabilization and control moment gyroscope (CMG) stabilization. Dynamic stabilization utilizes tactical steering techniques to trigger a lean in the vehicle in the intended direction for balancing, while CMG stabilization employs the reactive precession torque of a high speed flywheel about an axis that will act to balance the vehicle. Of these two, CMG stabilization offers greater advantages for static vehicles. This paper proposes a first order sliding mode controller (SMC) design to control the CMG and stabilize a bicycle at zero-forward velocity. This study also compares the SMC method to a PID controller to validate the advantages of the SMC controller for the highly non-linear system dynamics of static stabilization. The result of two experimental setups are presented and discussed. The first experimental platform is a single degree of freedom (DOF) inverted pendulum and the second is a three DOF bicycle.**

I. INTRODUCTION

A. History of Autonomous Stabilization

Attempts at autonomous stabilization of inherently unstable vehicles have dated back to the early 20th century. In 1905, Louis Brennan built a Gyroscopic Monorail that utilized a CMG system controlled by passive actuation of several mechanisms and mechanical sensors designed to respond to the monorail's tilt orientation. The monorail successfully executed test runs carrying 50 passengers along a circular path [1]; however, due to the limited accuracy of sensors and robust controllers at that time it was more practical to employ inherently stable two rail systems. In 1909 and 1911 similar projects where endeavored by Scherl and Shilovsky [2]. Shilovsky's gyrocar was a two wheeled vehicle with the wheels oriented in tandem. The gyrocar was capable of being manually stabilized via a clutch activated CMG system, requiring the human passenger to actuate the clutch appropriately to gimbal the CMG's flywheel. Lack of sensors for accurate angular position, velocity, and acceleration feedback limited the autonomy of these early attempts. Today, much progress has been made in sensor technology, motor technology, control methods, and autonomous controllers making the use of a CMG stabilized 2-wheeled vehicle more practical.

In the advent of computer aided programs and microcontrollers, more research has been conducted on the self-stabilization of bicycles. Bicycle dynamics and control have been investigated in detail by Sharp [3]. The majority of these studies utilize dynamic stabilization where the bicycle is actively steered to induce leans that oppose the bicycle's instabilities while moving forward at a constant velocity; however, this attempt fails at stabilizing a static bicycle, a difficult task for human riders, because the passive gyroscopic stabilizing effect produced by the angular momentum of the bicycle's wheels is absent. A few different approaches have been pursued to achieve static stabilization, the most notable of which include: adding a rotor mounted on the crossbar [4], mounting a pendulum to balance the tilting force [5], and using the precession effects of a gyroscopic actuator [6], [7].

B. Research Focus

In this paper, a high speed flywheel with a single DOF gimbal is used to induce the torque that will counteract the moment due to gravity applied on the bicycle when it deviates or tilts from its semi-stable, vertical position. By applying a gimbal torque to a spinning flywheel, a simultaneous, amplified reactive torque is generated about an axis orthogonal to both the flywheel's gimbal axis and spin axis. This controllable reactive torque can be oriented to act about the axis that will balance an unstable bicycle.

This paper focuses on the control dynamics of a static bicycle and presents the experimental test results for two separate test platforms. The first experimental test platform was a single DOF inverted pendulum frame. Its mobility was constrained to rotation about just one axis with one revolute joint at its base. The second experimental test platform was a three DOF bicycle that can rotate about all three principle axes; however, due to friction between the tires and the ground, rotation of the bicycle will be predominantly about the bicycle's balancing axis. Rotation about the axis that would generate a 'wheelie' would never occur because the maximum reactive torque of the flywheel used was not large enough to lift the front or back wheel of the bicycle off the ground. For these reasons, the three DOF bicycle can be modeled using the same single DOF dynamic equations of motion as the pendulum. Stabilizing the bicycle adds to this study by testing a body whose geometric parameters are more similar to that of a vehicle, where the bicycle is not fully constrained to rotation about just one axis.

The outline of this paper is as follows. In Section 2, the reference coordinate system is introduced, the equations of motion are derived and all the assumptions used are listed. Section 3 provides a brief introduction to sliding mode controllers, and elaborates on the stabilization controller design. Section 4 presents the experimental results, and Section 5 offers concluding thoughts regarding the proposed controller.

[†] The Department of Electrical and Computer Engineering, The Ohio State University, Columbus, OH 43210, USA yetkin.2@osu.edu, ozguner.1@ece.osu.edu

[‡] The Department of Mechanical and Aerospace Engineering, The Ohio State University, Columbus, OH 43210, USA kalouche.2@osu.edu

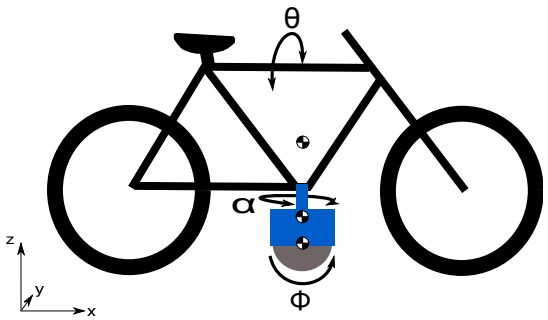

Fig. 1: Free body diagram of the bicycle model

TABLE I: Parameters for Static Bicycle

Parameter	Symbol
Bicycle mass & height of c.m	m_b & h_b
Gyro mass & height of c.m	m_g & h_g
Flywheel mass & height of c.m	m_f & h_f
Flywheel spin velocity	Ω
Gravity constant	g
Bicycle Inertia	I_{b_x}
Gyro Inertia	$[I_{g_x}, I_{g_y}, I_{g_z}]$
Flywheel Inertia	$[I_{f_x}, I_{f_y}, I_{f_z}]$

II. Bicycle Dynamics

A. Coordinates and Assumptions

The coordinates of the bicycle are defined as:

- θ - Roll angle
- α - Gimbal angle
- Φ - Flywheel spin direction

Fig. 1 shows a simplified sketch of the bicycle. The bicycle is composed of three rigid bodies:

- The bicycle frame with the wheels
- The gyroscope without the flywheel
- The flywheel

Here, the flywheel and the gyro are considered two different rigid bodies since the flywheel also spins along the y-axis while the gyro does not. The full list of parameters used to derive the equations are given in Table I.

In order to derive the equations of motion for the bicycle, the following assumptions are considered

- Tires have zero width
- No slipping force applied to the bicycle's tires
- All three rigid bodies are taken as point masses at their center of gravity

B. Equations of Motion

The nonlinear dynamics of these three rigid bodies were derived from conservation of energy by using Lagrange's method. Define L such that

$$L = T - U \tag{1}$$

where T is the kinetic energy, and U is the potential energy of the system. The kinetic and potential energy equations were derived for the bicycle frame, the gyro, and the flywheel.

$$T = T_{Bicycle} + T_{Gyro} + T_{Fly} \quad U = (m_g h_g + m_b h_b + m_f h_f) g cos\theta \tag{2}$$

where

$$T_{Bike} = \frac{1}{2}\left(I_{b_x} + m_b h_b^2\right)\dot{\theta}^2 \tag{3}$$

$$T_{Gyro} = \frac{1}{2}\left(m_g h_g^2 \dot{\theta}^2 + I_{g_x}\dot{\theta}^2 cos^2\alpha + I_{g_y}\dot{\theta}^2 sin^2\alpha + I_{g_z}\dot{\alpha}^2\right) \tag{4}$$

$$T_{Fly} = \frac{1}{2}\left(m_f h_f^2 \dot{\theta}^2 + I_{f_x}\dot{\theta}^2 cos^2\alpha + I_{f_y}\left(\Omega + \dot{\theta}^2 sin^2\alpha\right) + I_{f_z}\dot{\alpha}^2\right) \tag{5}$$

Assuming a non-conservative disturbance force ($d(t)$) acting on the horizontal x-y plane, the equation of motions were derived from Euler-Lagrange equation

$$\frac{d}{dt}\left(\frac{\partial L}{\partial \dot{\theta}}\right) - \frac{\partial L}{\partial \theta} = d(t) h_b \sin\theta \tag{6}$$

giving the acceleration of the tilt angle as

$$\ddot{\theta} = \frac{K_1 g sin\theta + 2I_1 \dot{\theta}\dot{\alpha} sin\alpha cos\alpha - I_{f_y}\Omega cos\alpha\dot{\alpha} - d(t) h_b \sin\theta}{I_{b_x} + K_2 + \left(I_{g_x} + I_{f_x}\right) cos^2\alpha + \left(I_{g_y} + I_{f_y}\right) sin^2\alpha} \tag{7}$$

where

$$K_1 = m_b h_b + m_g h_g + m_f h_f \tag{8}$$

$$K_2 = m_b h_b^2 + m_g h_g^2 + m_f h_f^2 \tag{9}$$

$$I_1 = I_{g_x} + I_{f_x} - I_{g_y} - I_{f_y} \tag{10}$$

From (7), it can be seen that the precession effect created by the motion of the flywheel has a significant role in the upright stabilization of the bicycle. Furthermore, it can be concluded that as Ω increases the flywheel will be more resistant to a change in orientation and thus will be able to generate a larger reactive torque. This means that stabilization can be achieved at a greater initial tilt angle, or in the presence of larger disturbances.

III. Controller Design

A. Brief Introduction to Sliding Mode Control

Variable structure systems (VSS) have been an attractive research topic for more than half a century. The first approach of discontinuous control was in the form of a bang-bang controller [8]. After [9], the VSS and sliding mode control theory gained significant interest from both researchers and engineers. Utkin and Young designed a sliding manifold to ensure optimality by using the pole

placement technique [10]. Su, Drakunov, and Ozguner [11] studied the problem of constructing discontinuity surfaces from a Lyapunov point of view which is also applicable on nonlinear systems.

The chattering phenomena, the major drawback of the sliding mode control method, was also studied by many researchers and several different approaches have been taken to reduce the chattering. In [12], the switching function is replaced with a continuous approximation in the vicinity of sliding manifold; however, the robustness of the sliding mode remained an issue. Young and Ozguner [13] proposed two design methods, one was based on pole placement, and the other was based on frequency-shaped quadratic optimal control formulation. This proved to reduce the chattering while preserving the insensitivity of the sliding mode against the uncertainties.

The major advantages of sliding mode control are [14]

- An exact model is not required to apply control to the system since sliding mode control is insensitive to unmodeled dynamics and disturbances
- The complexity of the feedback design is reduced
- It is a nonlinear control method
- It can be applied to a wide range of problems in robotics, electric drives, and vehicle and motion control

B. Design of Sliding Mode Controller

In order to design a controller to achieve the upright stabilization of the bicycle, a nonlinear state space model of the system was needed. From the equation of motion in (7), varying the gimbal angle (α) the precession torque is induced, which stabilizes the bicycle. However, assigning the gimbal angle as the control input causes the relative degree of the system become greater than one [15]. Hence, the rate of the gimbal angle ($u = \dot{\alpha}$) is chosen as the control input of the system dynamics, and it is integrated over time before the actual control is applied to the motor.

The following nonlinear state space model summarizes the system dynamics from a control point of view:

$$\ddot{\theta} = f(\theta, \dot{\theta}, \alpha) + g(u, \dot{\theta}) \tag{11}$$

$$y = [\theta, \alpha] \tag{12}$$

where

$$f = \frac{K_1 g \sin\theta + f_d h_b \sin\theta}{I_{b_x} + K_2 + \left(I_{g_x} + I_{f_x}\right) cos^2\alpha + \left(I_{g_y} + I_{f_y}\right) sin^2\alpha} \tag{13}$$

$$g = \frac{2I_1 \dot{\theta} \sin\alpha\cos\alpha - I_{f_y}\Omega\cos\alpha}{I_{b_x} + K_2 + \left(I_{g_x} + I_{f_x}\right) cos^2\alpha + \left(I_{g_y} + I_{f_y}\right) sin^2\alpha} u \tag{14}$$

Here, f_d represents the disturbance and unmodeled system dynamics.

To find the sliding mode controller gains, the following surface equation is considered:

$$s = c_1\theta + \dot{\theta} \tag{15}$$

The derivative of the surface equation is taken.

$$\dot{s} = c_1\dot{\theta} + \ddot{\theta} \tag{16}$$

$$\begin{aligned} h(\alpha)\dot{s} = {} & h(\alpha)c_1\dot{\theta} + (K_1 g + f_d h_b)\sin\theta \\ & + \left(2I_1\dot{\theta}\sin\alpha\cos\alpha - I_{f_y}\Omega\cos\alpha\right) u \end{aligned} \tag{17}$$

where $h(\alpha)$ represents the denominator of $\ddot{\theta}$. Then, by selecting the control in the form of

$$u = -|k_1\theta + k_2\dot{\theta}|sign(s) \tag{18}$$

the relation between s and $\dot{s}$ is obtained as

$$h(\alpha)\dot{s} = h(\alpha)c_1\dot{\theta} + (K_1 g + f_d h_b)\sin\theta \tag{19}$$

$$+ \left(2I_1\dot{\theta}\sin\alpha\cos\alpha - I_{f_y}\Omega\cos\alpha\right)|k_1\theta + k_2\dot{\theta}|sign(s) \tag{20}$$

After linearizing $\sin\theta = \theta$ which remains valid for $|\theta| <$ 30 degree, and taking the upper bounds of the nonlinear terms and the uncertainties in (20), the equation becomes

$$H\dot{s} = Hc_1\dot{\theta} + (K_1 g + f_0 h_b)\,\theta \tag{21}$$

$$+ \left(2I_1\dot{\theta} - I_{f_y}\Omega\right)|k_1\theta + k_2\dot{\theta}|sign(s) \tag{22}$$

where H is the constant value of $h(\alpha)$ at the upper bound of the nonlinear terms. Global asymptotic stability will be ensured when the reachability condition (23) is satisfied.

$$\begin{aligned} \dot{s} < 0 \qquad & \leftarrow sign(s) > 0 \\ \dot{s} > 0 \qquad & \leftarrow sign(s) < 0 \end{aligned} \tag{23}$$

Hence, selecting the control gains as the following will satisfy the reachability condition and guarantee stability. [14] gives further information about the asymptotic stability of sliding mode controllers.

$$k_1 > \left|\frac{K_1 g + f_0 h_b}{2I_1\dot{\theta}_0 - I_{f_y}\Omega}\right| \qquad \text{and} \qquad k_2 > \left|\frac{Hc_1}{2I_1\dot{\theta}_0 - I_{f_y}\Omega}\right| \tag{24}$$

where, $\dot{\theta}_0$ represents the upper bound of the rate of the tilt angle.

IV. Experimental Results

Experimental results were obtained on two different test platforms, an inverted pendulum and a bicycle shown in Fig. 2 and Fig. 3, respectively. Fig. 2 also shows a close up view of the gyro and flywheel.

On the inverted pendulum setup, an encoder was used to measure the tilt angle to obtain precise tilt angle measurements. On the bicycle setup, an Inertial Measurement Unit (IMU) was utilized in lieu of an encoder. This results in oscillatory balancing of the bicycle.

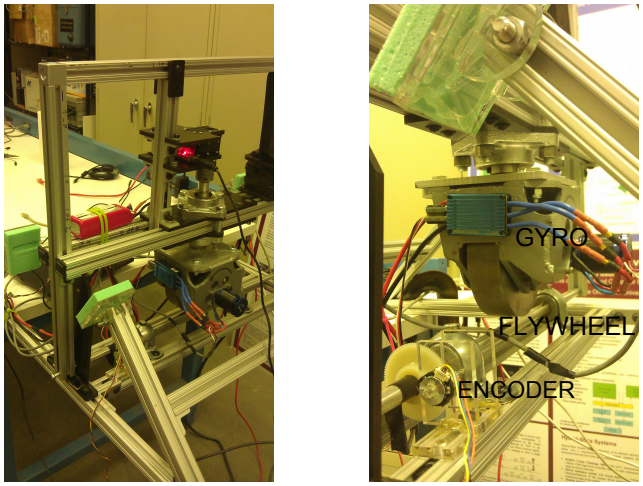

(a) (b)

Fig. 2: Inverted Pendulum setup a) View of inverted pendulum. b) Close-up view of gyro and flywheel.

TABLE II: Parameter Values for Experimental Setups

Parameter	IP Setup Value	Bicycle Setup Value	Unit
$[m_b, m_g, m_f]$	$[6.2, 2.23, 2.88]$	$[14, 2.23, 2.88]$	[kg]
$[h_b, h_g, h_f]$	$[18, 12.6, 8.3]$	$[23, 14, 9.7]$	[cm]
Ω	1000	1500	[rad/sec]
I_{b_x}	2129	10200	[kg cm^2]
$[I_{g_x}, I_{g_y}]$	[39, 60]	[39, 60]	[kg cm^2]
$[I_{f_x}, I_{f_y}]$	[28.5, 30.2]	[28.5 30.2]	[kg cm^2]

Fig. 3: Bicycle setup

A. Experimental Results Obtained on Inverted Pendulum Setup

The control input (18) for the inverted pendulum was found by picking coefficients (24) based on parameter values shown in II. The coefficients of the sliding surface (15) were selected proportional to the importance of their associated values. The final control input was given as:

$$u = |9\theta + 2\dot{\theta}|sign(6\theta + \dot{\theta}) \tag{25}$$

From (25), it is seen that the gimbal angle is not a controlled variable. However, due to the fact that the utilized servo motor has a turn range of $(\pm 126^\circ)$, it is advised to bring the gimbal angle back to its equilibrium point. Otherwise, in cases where the gimbal angle reaches its boundary, and a disturbance is applied to the pendulum, the motor will turn no more and consequently no more torque will be generated, which causes the pendulum to fall over. To overcome such issues, after stabilization is achieved by applying the control input in (25), the gimbal angle is taken back to zero without disturbing the pendulum's stability by applying the following control input:

$$u = -c_\alpha \frac{sign(\alpha)}{|\cos\alpha|} \tag{26}$$

Here, c_α is a coefficient which determines the speed of the gimbal angle's convergence to zero at the risk of disturbing the pendulum's stability. Experimentally, it is found that the controller performs better at taking the gimbal angle back to zero when $c_\alpha = 0.01$. During this process, if the stability of the pendulum was disturbed by an external force or by the torque generated during the process, the control in (25) was again applied until stability was reached.

Fig. 5 shows the experimental results obtained on the inverted pendulum setup, with the initial tilt angle set to $\theta(0) = -18[deg]$. The results show that the proposed control method successfully stabilizes the pendulum at its equilibrium point, and brings the gimbal angle back to zero without affecting the stability of the system. The latter process takes place between $t = 5$sec and $t = 27$sec. The results also show that there was a stability region of ± 0.3 degree due to the friction between the revolute joint of the pendulum and the base.

In order to test the robustness of the controller, a horizontal force of 6.1kg m/s^2 was applied to the system along the y-axis for 2.5 seconds. This was equivalent to an impulse of 15.26 kg m/s. Fig 6 shows the that while the pendulum is vertically stable, a disturbance is applied at $t = 10$ seconds. The gimbal angle was rotated to the opposite side to counteract the disturbance, which returns the pendulum back to zero.

The performance of the proposed controller design also needed to be verified. In order to test this, a simple PID controller was also applied to the system. The PID controller was constructed as

$$u = K_P e(t) + K_D \frac{d}{dt} e(t) + K_I \int e(\tau) d\tau \tag{27}$$

where K_P, K_D, and K_I are proportional, derivative, and integrator gains, and $e(t)$ is the difference between the current tilt angle and the desired angle ($\theta_{\text{des}} = 0$). After various trials, the best results are obtained for the following gain values:

$$K_P = 6 \qquad K_D = 2 \qquad K_I = 2 \tag{28}$$

These two controller methods are compared by setting the same initial tilt angles and flywheel rotational velocity, and observing the performance of the controllers for multiple, consecutive tests.

Fig. 7 shows that the rising and settling times of sliding mode controller are approximately 0.5 seconds and 10 seconds shorter than those of this PID controller. In addition,

while 4-7 degrees of overshoot was observed using the PID controller, the SMC applied experiments had almost no overshoot. Hence, it can be concluded that sliding mode controller performs better compared to this PID controller.

B. Experimental Results Obtained on Bicycle Setup

The major challenge of the controller implementation of the bicycle setup compared to the inverted pendulum was that an IMU was used to measure the tilt angle. This sensor introduced time delayed measurements that were susceptible to the vibration and magnetic field generated by the spinning ferrous flywheel and motors. These inaccuracies coupled with the round shape of the tires caused oscillations in the tilt angle during stabilization.

Due to different system parameters, a different control input was found:

$$u = |14\theta + 3\dot{\theta}|sign(6\theta + \dot{\theta}) \tag{29}$$

Fig 4 shows the results obtained on the bicycle setup.

Due to the increased weight of the bicycle, a smaller initial tilt angle of 5 degrees was used. In addition, a greater angle of 30 degrees for the gimballing servo motor was used to provide a longer time for applying usable torque. The results display that the bicycle keeps oscillating between ± 1 degree due to the above limitations.

V. CONCLUSIONS

In this attempt to validate the robust capabilities of control moment gyroscope (CMG) stabilization, a first order sliding mode controller was developed and implemented on two physical test beds. A second, PID controller, was also designed and tested on the inverted pendulum platform as a means to evaluate the performance characteristics of the SMC. Of these two controllers, the SMC proved to be advantageous for stabilization by offering reduced overshoot and shorter rising and settling times. The first experimental setup was a single DOF mechanism that was free to rotate about a fixed revolute joint. This platform could be accurately modeled as an inverted pendulum constrained from translation about three axes and rotation about two axes. The second setup, a three DOF bicycle, more closely resembles the geometry of a vehicle but can be modeled as a single DOF system for static stabilization tests. The experimental test results obtained on both test beds validate that CMG stabilization of a single-axis gimbal flywheel can be used to actively control and stabilize inherently unstable bodies (e.g. inverted pendulums, bicycles, motorcycles, etc.). This study validates the feasibility and robust capabilities of CMG stabilization for these systems. Future vehicles using CMG stabilization can be designed to offer unparalled stability and manueverability across rugged off-road terrains as well as on streets for transportation purposes. A two wheeled street vehicle can weigh less than a four wheeled vehicle and can therefore advantageously reduce energy consumption of the vehicle.

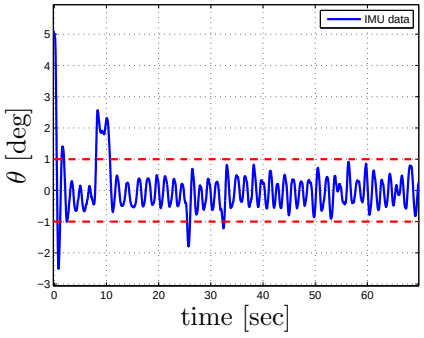

Fig. 4: Experimental results showing the bicycle is stabilized.

ACKNOWLEDGMENT

The authors would like to thank Codrin-Gruie Cantemir and Daniel Kestner for their help with the understanding of the system dynamics and construction of the experimental setups.

REFERENCES

[1] L. G. Brennan, "Nasal splint device," Jun. 11 1991, uS Patent 5,022,389.

[2] P. Schilowsky, Oct. 15 1912, uS Patent 1,041,680.

[3] R. S. Sharp, "The stability and control of motorcycles," *Journal of mechanical engineering science*, vol. 13, no. 5, pp. 316–329, 1971.

[4] Y. Yavin, "Stabilization and control of the motion of an autonomous bicycle by using a rotor for the tilting moment," *Computer methods in applied mechanics and engineering*, vol. 178, no. 3, pp. 233–243, 1999.

[5] S. Lee and W. Ham, "Self stabilizing strategy in tracking control of unmanned electric bicycle with mass balance," in *Intelligent Robots and Systems, 2002. IEEE/RSJ International Conference on*, vol. 3. IEEE, 2002, pp. 2200–2205.

[6] A. Beznos, A. Formal'sky, E. Gurfinkel, D. Jicharev, A. Lensky, K. Savitsky, and L. Tchesalin, "Control of autonomous motion of two-wheel bicycle with gyroscopic stabilisation," in *Robotics and Automation, 1998. Proceedings. 1998 IEEE International Conference on*, vol. 3. IEEE, 1998, pp. 2670–2675.

[7] H. Yetkin and U. Ozguner, "Stabilizing control of an autonomous bicycle," in *Control Conference (ASCC), 2013 9th Asian*. IEEE, 2013, pp. 1–6.

[8] S. Emel'Yanov and N. Kostyleva, "Some peculiarities in the motion of variable-structure automatic control systems with discontinuous switching functions," in *Soviet Physics Doklady*, vol. 8, 1964, p. 1152.

[9] V. Utkin, "Variable structure systems with sliding modes," *Automatic Control, IEEE Transactions on*, vol. 22, no. 2, pp. 212–222, 1977.

[10] V. I. Utkin, "Methods for constructing discontinuity planes in multidimensional variable structure systems," *Automation and Remote Control*, vol. 39, pp. 1466–1470, 1978.

[11] W.-C. Su, S. V. Drakunov, and Ü. Özgüner, "Constructing discontinuity surfaces for variable structure systems: a lyapunov approach," *Automatica*, vol. 32, no. 6, pp. 925–928, 1996.

[12] H. Kwatny and T. Siu, "Chattering in variable structure feedback systems," *Automatic control*, pp. 307–314, 1988.

[13] K. David Young and Ü. Özgüner, "Frequency shaping compensator design for sliding mode," *International Journal of Control*, vol. 57, no. 5, pp. 1005–1019, 1993.

[14] V. I. Utkin, "Sliding mode control," *Variable structure systems: from principles to implementation*, vol. 66, p. 1, 2004.

[15] H. K. Khalil, *Nonlinear systems*. Prentice hall Upper Saddle River, 2002, vol. 3.

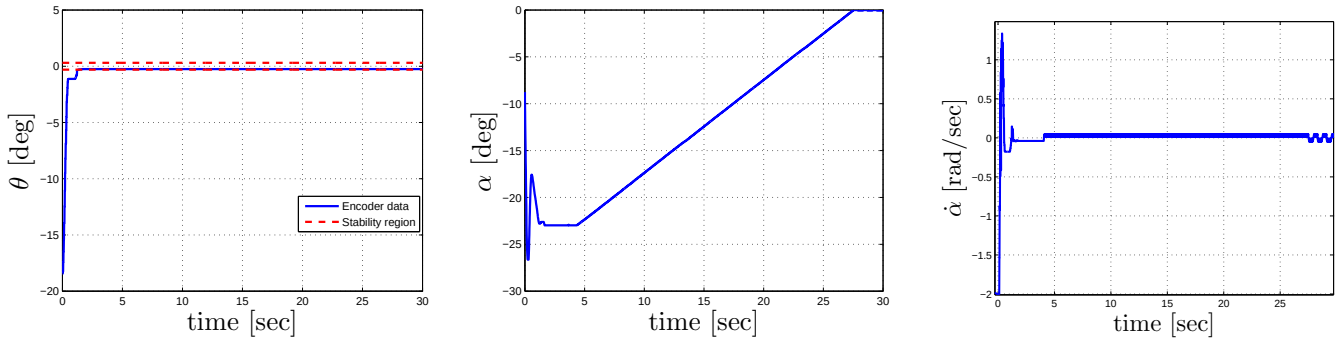

(a) (b) (c)

Fig. 5: Experimental results showing the pendulum is stabilized. (a) - Tilt angle measured with encoder (b) - Gimbal angle (c) - Control input

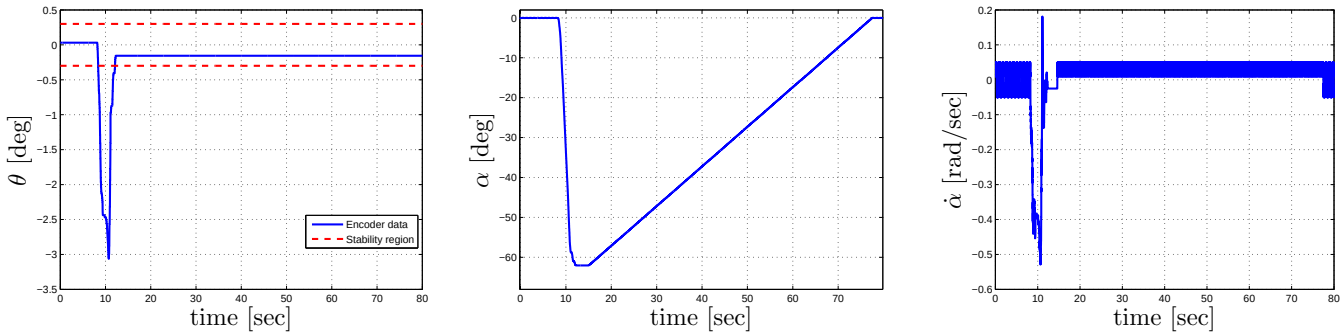

(a) (b) (c)

Fig. 6: Experimental results for first measured disturbance. (a) - Tilt angle measured with encoder (b) - Gimbal angle (c) - Control input

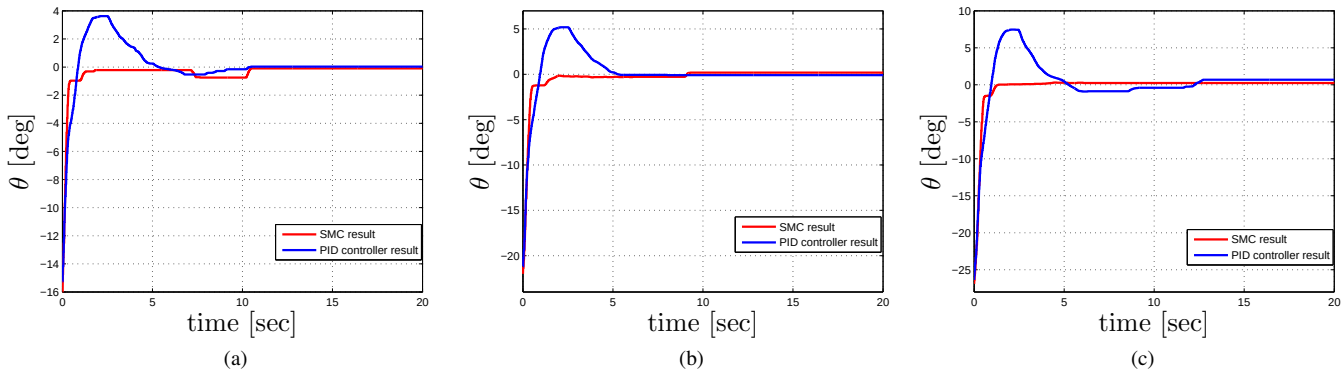

(a) (b) (c)

Fig. 7: Comparison of SMC and PID for the same initial tilt angles. (a) - Initial tilt angle is -16 degrees (b) - Initial tilt angle is -21 degrees (c) - Initial tilt angle is -26 degrees